

Long-distance and high-impact wind farm wake effects revealed by SAR: a global-scale study

Rui Li¹, Jincheng Zhang¹ and Xiaowei Zhao^{1*}

¹Intelligent Control & Smart Energy (ICSE) Research Group,
School of Engineering, University of Warwick, Coventry, UK.

*Corresponding author(s). E-mail(s):
xiaowei.zhao@warwick.ac.uk;

Contributing authors: rui.li.4@warwick.ac.uk;
jincheng.zhang.1@warwick.ac.uk;

Abstract

Wind, as a clean and sustainable source of energy, has witnessed significant growth in recent years. However, with a growing number of wind farms authorised, constructed and commissioned, the wake effect (the reduced wind speed caused by upstream wind farms) is emerging as a pressing concern for both farm owners and policymakers. Here, to systematically and comprehensively investigate the wake effects in real-world wind farms, we analyse the wind speed retrieved from 7122 Sentinel 1A/B SAR images spanning over three years, encompassing more than 60 large-scale wind farms across Europe and Asia. Our study reveals that long-distance wakes can propagate more than 100 km. Additionally, we identify that wake effects lead to, on average, a 1.204 m/s (or 12.4%) speed reduction for downstream wake-affected areas. We envisage that our quantitative findings can provide vital support to wake-related planning and legislation for future wind energy projects where wind power plants are expected to be in close proximity.

Keywords: wake effects, wind energy, remote sensing, wind farm, SAR

2 Long-distance and high-impact wind farm wake effects revealed by SAR

1 Main

Offshore wind farms are under sustained and accelerated development in recent years, driven by the soaring energy prices across the globe and the imminent net-zero target to tackle climate change [1–3]. When selecting an appropriate site for constructing a new wind farm, various design factors should be considered, including wind resource potential, initial construction cost, operation and maintenance expenses and proximity to transmission lines and roads [4]. However, finding sea areas that meet all these requirements can be challenging. Consequently, existing and under-construction wind farms often cluster together in sea areas with favourable conditions. For example, dozens of large-scale wind farms owned by different countries are already operating in North Sea, with more farms planned for the future. As these sea areas become increasingly crowded, it is crucial to consider and quantify the wake effects, which refer to the reduction in wind speeds in the downstream region caused by upstream wind farms. Understanding and addressing these wake effects are essential to navigate legal issues and conflicts that will inevitably arise from uncoordinated wind farm development in the foreseeable future, thereby enhancing the sustainability in wind energy planning and utilization [5, 6].

Wind farm wakes, as a complex aerodynamic phenomenon, are influenced by many factors such as upstream wind speeds, atmospheric stability and meteorological conditions. Currently, two mainstream technologies are used to investigate the potential impacts of wake effects: mesoscale simulations [7–11] and in-situ measurements [12–16]. However, mesoscale simulations cannot encompass all operating conditions, limiting their ability to investigate wind farm wakes in real-world operational scenarios. On the other hand, in-situ measurements can only cover limited spatial areas and temporal durations. With existing technologies, it remains unclear (1) how far wind farm wakes can persist for real-world wind farm clusters and (2) to what extent the wakes generated by upstream wind farms can affect the power generation of downstream wind farms.

This study aims to address the aforementioned questions by utilizing Synthetic Aperture Radar (SAR) images to comprehensively investigate the impact of wind farm wakes. SAR images provide a reliable and universal means to analyze wind speeds in offshore environments, as the wind speed can be retrieved from these images using the C-band geophysical model function [17]. The reliability and consistency of SAR-derived wind speeds for offshore wind farms under both free-stream and wake conditions have been previously validated [18]. SAR images, captured by satellite-borne sensors, offer the advantage of global coverage, enabling the characterization of wakes in wind farms worldwide with high fidelity. Although SAR images have been used to investigate wake effects in previous studies [9, 19–23], the scale of SAR data and the range of research areas have been limited, leaving the full potential of remote sensing technology untapped for wind energy applications. In this work, we collect a comprehensive dataset consisting of 7122 Sentinel 1A/B

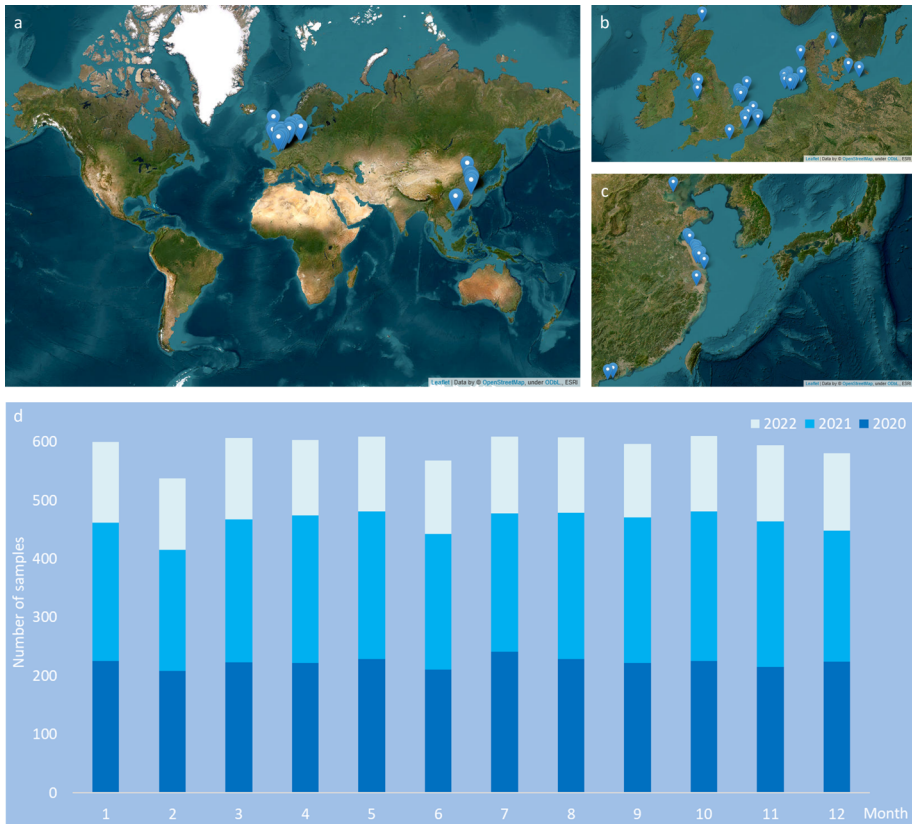


Fig. 1: The spatial and temporal distributions of the collected Sentinel 1A/B SAR images. (a) Locations of wind farms included in the collected data with (b) European part and (c) Asian part. (d) Monthly number of samples collected in three years.

SAR images, totalling more than 11.5 TB of data, obtained from the Copernicus Open Access Hub over a three-year period (2020–2022). These images cover over 60 offshore wind farms across Europe and Asia. The spatial and temporal distributions of the wind farms analyzed in this study are illustrated in Fig. 1. Only SAR images captured after the wind farms were fully commissioned are utilized to ensure a consistent evaluation. Furthermore, the data collection spans evenly all months of the year, as shown in Fig. 1(d), allowing for the examination of seasonal variations of wake behaviours. Based on the collected data, a processing pipeline is developed to retrieve the wind speed (Appendix A) while the accuracy is verified by the buoy data (Appendix B). Finally, an image-processing method is proposed to obtain the upstream freestream wind speeds and the downstream wake speeds (Appendix C). In addition, further enhancements to the whole procedure will be included in our future work,

4 Long-distance and high-impact wind farm wake effects revealed by SAR

including the advanced wind speed vertical extrapolation (Appendix D) and high-resolution wind direction (Appendix E).

Based on the analysis of SAR images obtained from over 60 wind farms across Europe and Asia during the years 2020, 2021, and 2022, two findings regarding wind farm wake effects are presented in this study. Firstly, the study demonstrates that wake effects can extend more than 100 km. The extended wake range has important implications for wind farm planning and development. Secondly, the study reveals that on average, wind farm wake effects lead to a 12.4% reduction in wind speed in downstream wake-affected sea areas. This reduction in wind speed has a direct impact on the power generation potential of downstream wind farms, highlighting the economic impact of wake effects.

The wind farm wake effects have significant economic implications globally and are acknowledged as a crucial concern by both academia and industry. However, neither the government nor the wind energy industry has yet to establish a settlement or legislation to compensate downstream wind farms for the revenue loss caused by upstream wind farm wakes [4, 5]. This lack of consensus can be attributed, in part, to the absence of a measurable and quantifiable index to assess the real economic impact of wake effects. The evidence provided by this work from SAR-derived wake loss assessment may accelerate the policy-making processes through providing technical support to address such issues.

2 Long-distance wakes confirmed by SAR

Early research utilizing SAR data has provided evidence that wind farm wakes can persist for more than 20 km downstream [19]. Mesoscale studies using the Weather Research and Forecasting (WRF) model have also shown velocity deficits in downstream areas at distances of at least 15 km from upstream wind farms [24]. However, with the increase in turbine size and farm scale, there is mounting evidence that estimates of 15 km or 20 km for wake propagation are no longer valid. In-situ measurements conducted over wind farms in the German Bight, such as Amrumbank West and Godewind, confirm that wake effects can extend at least 45 km downwind [12]. Qualitative studies based on SAR images have also revealed that wakes can extend over 50 km [25, 26]. In the case of superimposed wakes behind multiple wind farms, the wake length can reach distances of up to 70 km, as observed in SAR images [27]. The recent mesoscale simulation research further demonstrates that wakes can extend up to 90 km downwind in certain flow conditions [28].

Currently, the recovery of low momentum and high turbulence caused by upstream wind farms is deemed to require a distance of at least 50 km [4]. However, our study, based on SAR-retrieved wind speed, unveils the frequent occurrences of long-distance wakes persisting up to 100 km downstream in the real world, as shown in Fig. 2. These long-distance wakes were captured in North Sea at various times over a three-year period. The details of wind farms

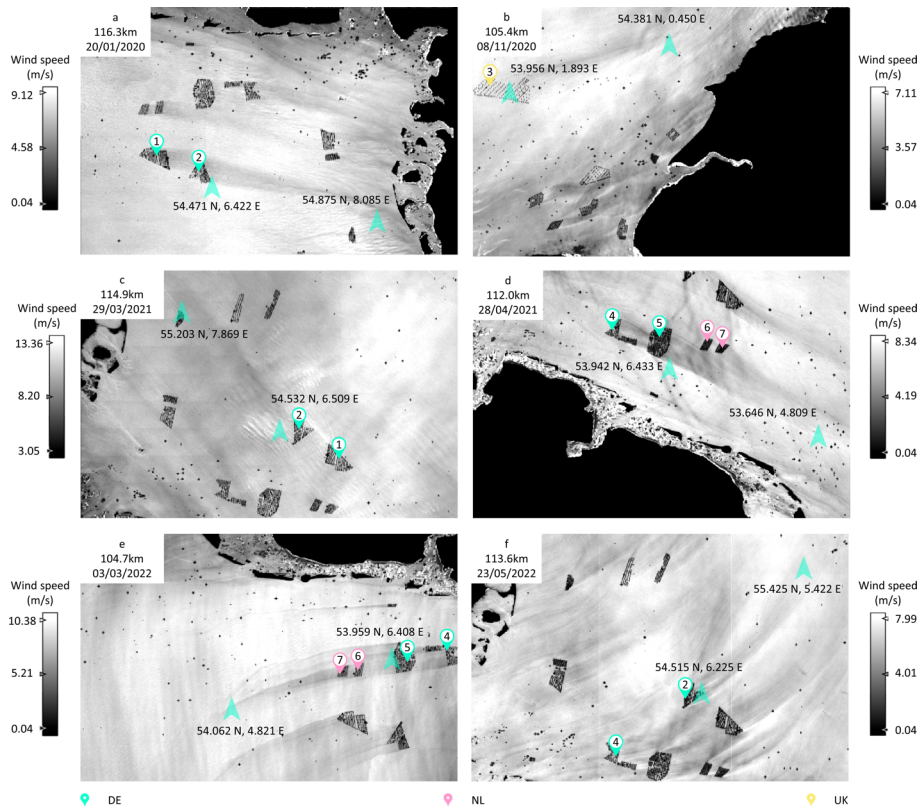
Long-distance and high-impact wind farm wake effects revealed by SAR

Fig. 2: Wake effects can extend up to 100 km, as indicated by the blue arrows in the figure. The propagation distance, shown in the second row of labels, is calculated based on the coordinates. The colour of the location symbol represents the operating country of the corresponding wind farm, as indicated in the legend at the bottom of the figure. For more information about the wind farms involved, please refer to Table 1.

involved can be found in Table 1. Specifically, panels (a), (c), (d), (e) and (f) of Fig. 2 were captured in the German Bight. The figures clearly demonstrate that superimposed wakes resulting from multiple wind farm clusters can extend as far as 116.3 km. Furthermore, even a single cluster with sufficient capacity can also generate wake effects that reach over 100 km. As shown in panel (b), the English Hornsea Project located off the Yorkshire coast, with its impressive capacity of over 2.6 GW, generates wake effects that extend downstream for an extraordinary distance of 105.4 km. Considering these long-distance wakes extending up to 100 km downstream, as revealed by our study, it becomes necessary to reconsider and potentially adjust the planning criteria for future wind projects, to account for these long-distance wake effects. The findings

6 *Long-distance and high-impact wind farm wake effects revealed by SAR***Table 1:** Information about wind farms contained in Fig. 2, including operating country, capacity (MW) and the number of turbines. In total, 18 wind farms belonging to three countries (DE, NL and UK) are included, with 1269 turbines and 7.80 GW capacity.

Number	Wind Farm Name	Country	Capacity (MW)	Turbines
1	Deutsche Bucht	DE	252	31
	Veja Mate	DE	402	67
	BARD Offshore 1	DE	400	80
2	Hohe See	DE	497	71
	Albatros	DE	112	16
	Global Tech I	DE	400	80
3	Hornsea Project One	UK	1218	174
	Hornsea Project Two	UK	1386	165
4	Nordsee One	DE	332.1	54
	Gode Wind 1	DE	330	55
	Gode Wind 2	DE	252	42
5	Trianel Windpark Borkum 1	DE	200	40
	Trianel Windpark Borkum 2	DE	203	32
	Borkum Riffgrund 1	DE	312	78
6	Borkum Riffgrund 2	DE	450	56
	Merkur	DE	396	66
	Alpha Ventus	DE	60	12
7	Gemini	NL	600	150

emphasize the importance of incorporating more comprehensive and accurate data on wake propagation in future wind farm planning processes.

Meanwhile, a significant number of large-scale wind farms are currently being constructed or planned within North Sea. For example, just around the wind farm cluster 1 in Fig. 2, nine wind farms ¹ with nearly 14 GW capacity are already under planning. At the same time, in the vicinity of cluster 2, two German wind farms ² with a combined capacity exceeding 2.4 GW are also under preliminary investigations. As shown in Fig. 2(a) and Fig. 2(c), the superimposed wakes caused by clusters 1 and 2 are already clearly visible and extend over a considerable distance. Upon completion of all the planned wind farms, with a capacity that is approximately nine times larger than the current capacity, the wake effects will cover a much wider geographical area and extend over a much greater distance. This substantial impact can have immediate economic repercussions and potentially hinder the development of future wind projects, reducing the sustainability of wind energy utilization. It becomes crucial to carefully consider and mitigate the potential challenges posed by these extended wake effects to ensure the sustainable growth and success of wind energy projects.

¹Doordewind I and Doordewind II of NL; Atlantis I, Nordlicht I, EnBW He Dreiht, N-9.1, N-9.2, N-9.3 and N-21.1 of DE

²N-10.1 and SEN-1

3 Pinpointing wake interactions by SAR

In addition to the long propagation distance of wind farm wakes, the velocity deficits caused by wind farm wakes are also substantial. For onshore wind farms, an estimated power generation loss of 5% has been observed, based on an econometric model and numerical weather prediction simulations [4]. Simulation studies for offshore wind farms have reported velocity deficits of 7% extending 100 km downstream and 10% extending 80 km downstream [29]. Real-world observations have shown persistent wake effects with velocity deficits of approximately 21% at a distance of 55 km downstream, while the speed loss can reach as high as 41% approximately 24 km downstream, as measured by LiDAR [21]. Wake effects can even be observed at 200 m altitude, albeit with smaller deficits compared to the hub height measurements [30].

Despite the extensive recognition and systematic investigation of wind farm wakes, the issue of justifying and quantifying their effects to resolve disputes between upstream and downstream wind farms remains unresolved [5, 6]. The absence of solid evidence to demonstrate the influence of wake effects is an urgent issue that needs to be addressed. While simulation results can suggest that wake effects may decrease productivity under certain conditions, they cannot prove the actual impacts on downstream wind farms in real-world operating scenarios, not to mention when and how these impacts occur. In contrast, SAR images offer a valuable and generic solution, as they capture wind speeds under real-world operating conditions, providing undeniable evidence of the actual impacts of wind farm wakes at specific timestamps.

Fig. 3 visually represents the wake interactions between adjacent wind farms. Panels (b), (c), and (d) demonstrate the wake interactions among wind farms within the same country, typically owned by different companies. In panel (b), the downstream wind farm clusters are entirely enveloped by the long-distance and high-impact wake effects generated by the upstream large-scale Hornsea Project. Medium-scale wind farms located in close proximity, as shown in panels (c) and (d), also experience significant wake interactions with each other. Resolving disputes between domestic wind farms can be relatively straightforward with the involvement of local authorities. However, complexities arise when wake interactions occur between wind farms owned by different countries, as evident in panels (a), (e), and (f). Taking panel (e) as an example, although three wind farm clusters are situated in their respective exclusive economic zones, the wake generated by clusters 1 (NL) and 2 (BE) clearly affects downstream cluster 3 (UK). Table 2 provides detailed information about the wind farms in Fig. 3, including those generating wakes and those influenced by wakes. It is noteworthy that a wind farm cluster can be both a culprit and a victim depending on the wind direction. Resolving transnational wake interactions requires bilateral and multilateral negotiation and cooperation to mitigate potential conflicts. Overall, the findings highlight that SAR images, with explicit timestamps and precise locations, effectively identify wind farm wakes and provide valuable insights into when and where these wake effects occur.

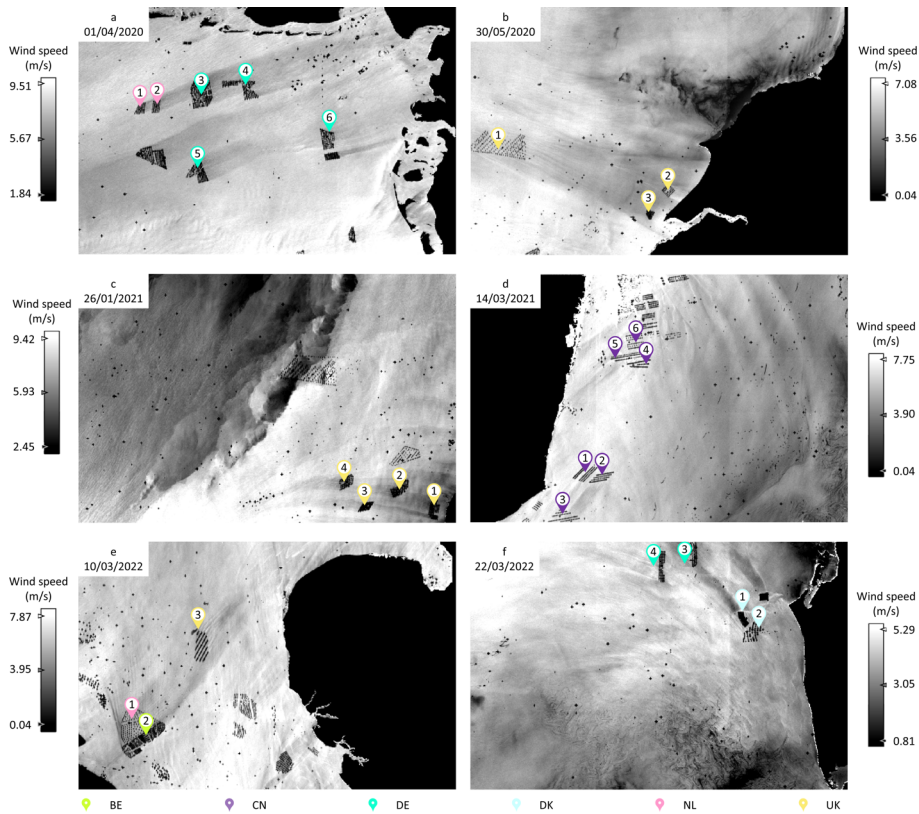


Fig. 3: Upstream wakes' impacts on the downstream wind farms, captured by SAR images with the explicit and precise timestamp (as shown in the top-left label). The colour of the location symbols corresponds to the operating country (refer to the legend at the bottom of the figure) of the respective wind farm. The SAR images are captured: (a) in German Bight; (b) near the coast of Holderness and Yorkshire; (c) near the coast of Lincolnshire; (d) in Yellow Sea near Jiangsu Province; (e) in North Sea between UK and NL; (f) near the Danish Jutland coast. For more detailed information about the wind farms involved, please refer to Table 2.

4 A first global-scale census on wake effects

After figuring out when and where wake effects take place, this section focuses on conducting extensive assessments to estimate the quantitative impact of wind farm wakes.

By utilizing the retrieved wind speed data (Appendix A) and identifying the upstream and wake-affected areas (Appendix C), this study accomplishes the first global-scale census on wind farm wake effects. Initially, cases with very small detected areas (often due to farms located at the edge of the SAR image) and extreme wind speeds (above 25 m/s or below 1 m/s) are filtered

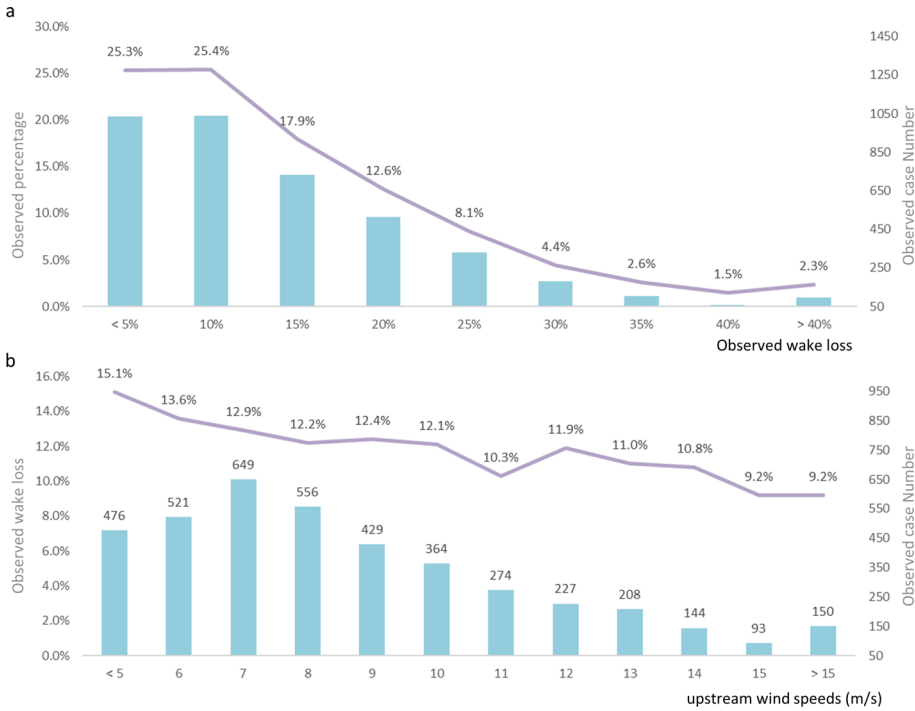


Fig. 4: (a) The distribution of different ranges of observed wake losses where the horizontal axis is the observed wake loss percentages. (b) The observed average wake losses under different upstream wind speeds where the horizontal axis is upstream wind speeds (m/s). For both charts, the bar graph is the number of samples.

out, resulting in 6335 samples for the subsequent quantitative assessment. Among all these samples, 4091 (64.6%) exhibit lower downstream wind speeds compared to the upstream wind speeds ³, indicating the presence of wake losses. The average velocity deficit for these samples is 1.204 m/s, which corresponds to a 12.4% reduction compared to the upstream wind speeds. Fig. 4(a) demonstrates that over half of the observed wake losses are below 10%, while approximately one-tenth of the samples experience wake losses exceeding 30%. Furthermore, Fig. 4(b) reveals a correlation between lower incoming wind speeds and increased wake-induced losses, consistent with in-situ measurement results [31]. This phenomenon will further exacerbate the already grave situation and pose additional challenges for wind farm operations, as wind farms inherently reduce the local wind speed [32], particularly as more and more farms are being built.

³As SAR is a real-world observation, there are multiple factors that account for reasons why the downstream wind speed is even higher than the upstream, such as the imaging quality, noise effect, side wind, retrieval quality and detection accuracy.

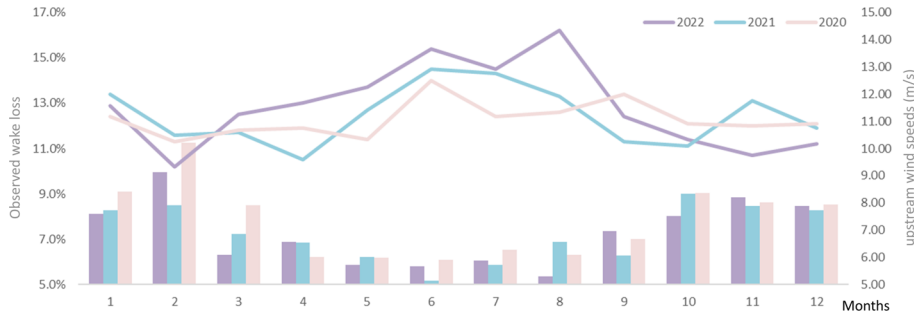


Fig. 5: The monthly average wake losses where the horizontal axis is the month. Please note that the line graph is the observed wake loss and the bar graph is the corresponding monthly average wind speed.

Next, the monthly observed wake losses during the three-year period are presented in Fig. 5. The line graph clearly shows that more wake losses are observed in the summer months compared to the winter months. To further analyze this finding, we calculate the corresponding monthly average wind speed of the study areas using the ERA5 hourly data [33]. The results are depicted in the bar graph of Fig. 5. It can be observed that the monthly average wind speed provides an explanation for the monthly distributions of the average wake-induced losses. Specifically, the monthly average wind speeds from April to September are noticeably lower than those from October to March. Considering the general trend that higher wind speeds are typically associated with lower wake losses (as demonstrated in Fig. 4(b)), it can be inferred that a more significant wake loss occurs during the summer months. It is important to note that all the analyzed wind farms are situated in the northern hemisphere especially in Europe and Asia, suggesting that this variation is likely specific to the region.

5 Discussion

This study confirms long-distance wakes propagating over 100 km in the real world. Furthermore, this research represents the first global-scale study to investigate over 4000 cases using SAR-derived wind speed data. The study covers more than 60 wind farms across the globe and spans a three-year duration from 2020 to 2022. The results reveal that the average velocity deficit caused by wake effects is 1.204 m/s, equivalent to 12.4% of the upstream wind speeds. The substantial evidence obtained in this work provides undeniable support for the frequent and significant impact of wind farm wakes. This is particularly pronounced in sea areas densely populated with wind farms, such as North Sea and Yellow Sea. These findings are expected to accelerate the progress of potential legislation and conflict resolution regarding wake-induced revenue losses between neighbouring wind farms in the foreseeable future.

At the same time, the long revisit time of the satellite is a major limitation of the SAR-based wake observation. Combining satellite observation and mesoscale simulation would be a potential direction in our future research.

Appendix A Wind speed retrieve from the SAR images

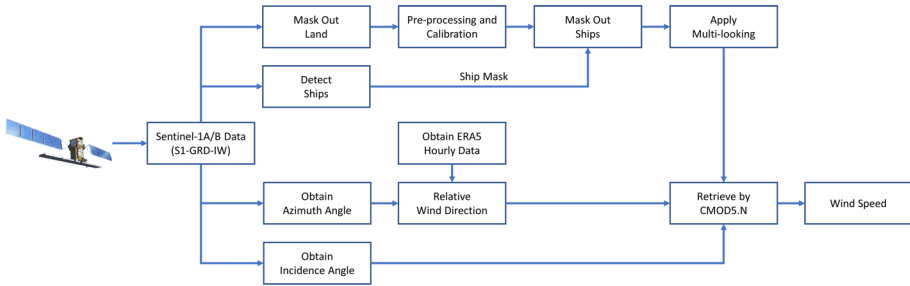


Fig. A1: The wind speed retrieval procedure.

In this study, we utilize the CMOD5.N algorithm [17] to retrieve wind speeds from the SAR images. The entire retrieval process is summarized in Fig. A1. Initially, we collect Sentinel-1A/B SAR images from the Copernicus Open Access Hub (<https://scihub.copernicus.eu/dhus/#/home>), with the product type being GRD and the sensor mode set to IW. Subsequently, we apply pre-processing and calibration using the SNAP toolbox (<http://step.esa.int/main>), including thermal noise removal, orbit correction, radiometric calibration and speckle noise filtering. Furthermore, we mask out land areas and remove bright objects like turbines and ships, as they tend to create strong radar reflections in the SAR image. The resulting images are then subjected to multi-looking, resulting in a final resolution of 500 meters. For wind speed retrieval using CMOD5.N, three external parameters are required: azimuth angle, incidence angle and wind direction. The first two parameters could be directly obtained from the SAR images themselves. Regarding wind direction, ERA5 hourly data (<https://www.ecmwf.int/en/forecasts/dataset/ecmwf-reanalysis-v5>) [33] are used as a reference. By combining all these procedures, the wind speed could be eventually retrieved from the SAR images.

Appendix B Verification of retrieved wind speed using buoy data

To assess the accuracy of the wind speed retrieved from the SAR images, we conduct a verification process using buoy data provided by the National Data Buoy Center (NDBC) (<https://www.ndbc.noaa.gov>). We collect data from six different NDBC buoy stations and corresponding SAR images from the same

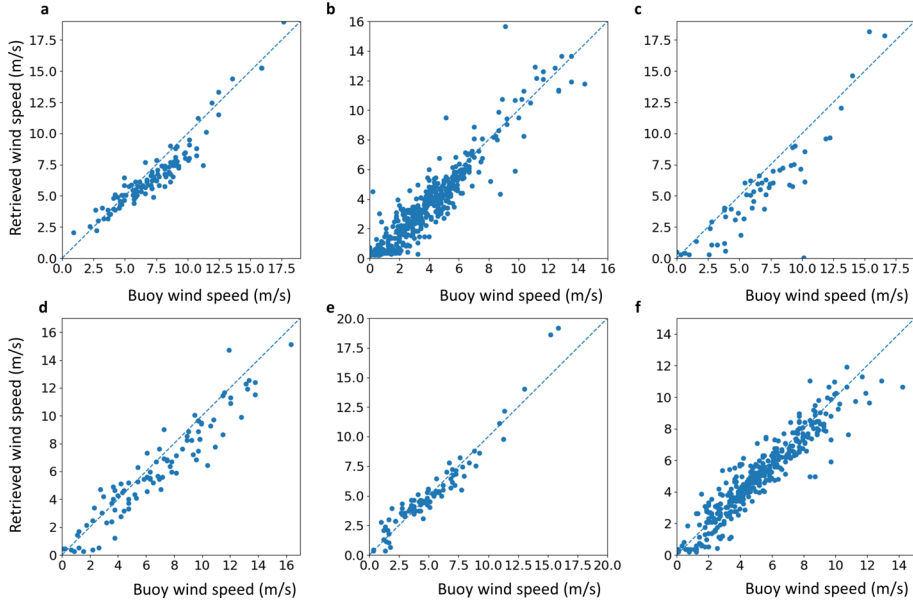


Fig. B1: The scatter plot of retrieved wind speed from Sentinel 1A/B using CMOD5.N relative to NDBC buoy wind speed.

locations spanning the period from 2020 to 2022. The buoy station IDs and their respective coordinates are as follows: 42020 (26.968N, 96.693W), 46025 (33.755N, 119.045W), 44009 (38.460N, 74.692W), 44007 (43.525N, 70.140W), 42036 (28.501N, 84.508W) and 46086 (32.499N, 118.052W). Next, we process the SAR images using our developed C-band model pipeline to retrieve the wind speed. We then extract the wind speed values at the corresponding buoy locations based on their coordinates and compare them to the buoy data. In total, we obtained 1165 matched pairs of buoy data and retrieved wind speeds (with 118, 434, 56, 96, 90 and 371 pairs for each station, respectively). Since most of the NDBC anemometers are installed at a height of 2.5–4 meters above the sea surface, we convert the measured speeds to the 10-meter neutral wind speeds using the method proposed by [34]. The scatter plots depicting the comparison results for the six cases can be seen in Fig. B1. More verification using advanced methods is still in progress.

Appendix C Upstream and downstream wind speed extraction

In this study, we develop an image processing method called Restricted-Region Gradient-Guided Growing (R^2G^3) to distinguish between the upstream free speed and the downstream wake speed from the retrieved wind speed data. The detailed parameters of the proposed R^2G^3 will be made publicly available

before publication. Some examples of detected farm, upstream area and wake-affected area by the proposed R²G³ are shown in Fig. C1.

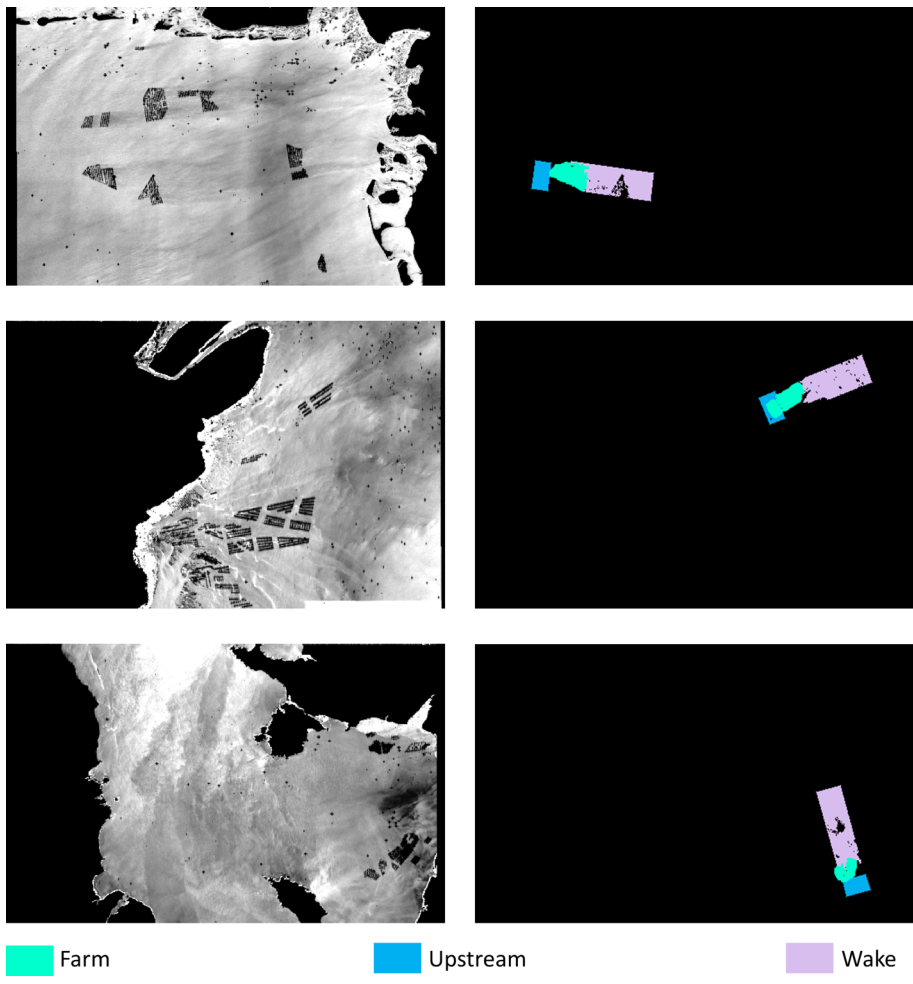


Fig. C1: Examples of detected farm, upstream area and wake-affected area by the proposed R²G³.

Appendix D Wind speed vertical extrapolation to hub height

The wind speed retrieved from Sentinel images is 10 m neutral wind speed, while the hub of wind turbines is typically around 100 m height. Therefore, the vertical extrapolation needs to be conducted to obtain the wind speed at 100

m height from the retrieved data. Two commonly employed techniques for this purpose are the power and logarithmic laws. The former demonstrates superior performance in unstable atmospheric conditions [35], whereas the latter is favoured in neutral atmospheric conditions [36]. In this version, we calculate the 100 m wind speed using the logarithmic laws [37]:

$$u(z_r) = \frac{\ln \frac{z_r}{z_0}}{\ln \frac{z}{z_0}} u(z), \quad (\text{D1})$$

where $u(z_r)$ and $u(z)$ represent the wind speeds at the height z_r and z , respectively. z_0 is the surface roughness, which was set to 0.0002 m [38]. In the future version, we will refine the wind speed extrapolation procedure such as by adopting advanced techniques e.g. [39].

Appendix E WRF simulation to downscale the wind direction.

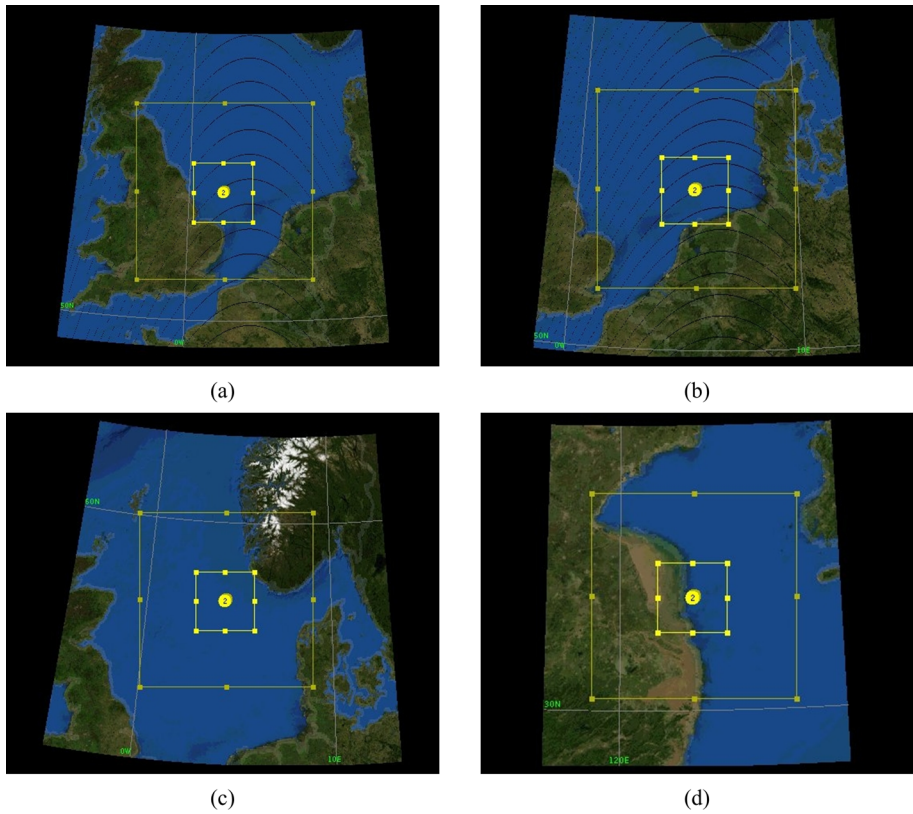


Fig. E1: Four example WRF simulation domains.

Especially, the wind direction is used as important information in the developed R²G³ to determine the upstream and downstream areas. However, the wind direction obtained from the ERA5 is rather coarse ($0.25^\circ \times 0.25^\circ$) for farm-level applications. To further improve the performance, the issue will be tackled by downscaling the resolution of Global Final Analysis (FNL) data using WRF v4.3.1 [40] in the future version. Four example simulation domains are shown in Fig. E1. Specifically, two domains are designed, where the resolutions of the outer domain and inner domain are $10\text{ km} \times 10\text{ km}$ and $2\text{ km} \times 2\text{ km}$, respectively. More details will be made publicly available when the paper is published.

Declarations

Acknowledgments. This work has received funding from the UK Engineering and Physical Sciences Research Council (grant number: EP/S000747/1). We express great appreciation to Copernicus Open Access Hub for providing the Sentinel images, Copernicus Climate Change Service for providing the ERA5 data, National Data Buoy Center for providing buoy measurement data, European Space Agency for providing the SNAP toolbox and National Center for Atmosphere Research for providing WRF and FNL data.

Data availability. The list of SAR images used in this study will be made publicly available before publication. The SAR data are available at the Copernicus Open Access Hub, <https://scihub.copernicus.eu/dhus/#/home>. The ERA5 data are available at the European Centre for Medium-Range Weather Forecasts, <https://www.ecmwf.int/en/forecasts/dataset/ecmwf-reanalysis-v5>. The buoy data are available at the National Data Buoy Center, <https://www.ndbc.noaa.gov>. The SNAP toolbox is available at Science Toolbox Exploitation Platform, <http://step.esa.int/main>. The WRF is available at National Center for Atmosphere Research, <https://www.mmm.ucar.edu/models/wrf>. The FNL data is available at NCAR Research Data Archive, <https://rda.ucar.edu/datasets/ds083.3>.

Code availability. Codes will be made publicly available before publication.

Author contributions. R.L. proposed and refined the concept, designed and implemented the whole processing framework including the SAR image processing, wind speed retrieval and verification, wake effects extraction and WRF simulation, designed and implemented the dataset analysis and visualization, and wrote the paper draft. J.Z. contributed to rendering the initial concept, analysing and interpreting the results, refining the wake extraction, and refining and editing the manuscript. X.Z. contributed to acquiring funding, analysing and interpreting the results, and refining and editing the manuscript. X.Z. supervised the overall study and investigation.

References

- [1] Perera, A., Javanroodi, K., Mauree, D., Nik, V.M., Florio, P., Hong, T., Chen, D.: Challenges resulting from urban density and climate change for the eu energy transition. *Nature Energy*, 1–16 (2023)
- [2] Howland, M.F., Quesada, J.B., Martínez, J.J.P., Larrañaga, F.P., Yadav, N., Chawla, J.S., Sivaram, V., Dabiri, J.O.: Collective wind farm operation based on a predictive model increases utility-scale energy production. *Nature Energy* **7**(9), 818–827 (2022)
- [3] Lei, Y., Wang, Z., Wang, D., Zhang, X., Che, H., Yue, X., Tian, C., Zhong, J., Li, L., Zhou, H., Xu, Y.: Co-benefits of carbon neutrality in enhancing and stabilizing solar and wind energy. *Nature Climate Change* (2023)
- [4] Lundquist, J.K., DuVivier, K.K., Kaffine, D., Tomaszewski, J.M.: Costs and consequences of wind turbine wake effects arising from uncoordinated wind energy development. *Nature Energy* **4**(1), 26–34 (2019)
- [5] Finseraas, E., Herrera Anchustegui, I., Cheynet, E., Guillermo Gebhardt, C., Reuder, J.: Gone with the wind? wind farm-induced wakes and regulatory gaps. Available at SSRN: <https://ssrn.com/abstract=4294614> or <http://dx.doi.org/10.2139/ssrn.4294614> (2022)
- [6] DuVivier, K., Mooney, B.T.: Moat mentality: Onshore and offshore approaches to wind waking. Available at SSRN: <https://ssrn.com/abstract=2718375> or <http://dx.doi.org/10.2139/ssrn.2718375> **1**, 1 (2020)
- [7] Fischereit, J., Brown, R., Larsén, X.G., Badger, J., Hawkes, G.: Review of mesoscale wind-farm parametrizations and their applications. *Boundary-Layer Meteorology* **182**(2), 175–224 (2022)
- [8] Larsén, X.G., Fischereit, J.: A case study of wind farm effects using two wake parameterizations in the weather research and forecasting (wrf) model (v3. 7.1) in the presence of low-level jets. *Geoscientific Model Development* **14**(6), 3141–3158 (2021)
- [9] Siedersleben, S.K., Lundquist, J.K., Platis, A., Bange, J., Bärfuss, K., Lampert, A., Cañadillas, B., Neumann, T., Emeis, S.: Micrometeorological impacts of offshore wind farms as seen in observations and simulations. *Environmental Research Letters* **13**(12), 124012 (2018)
- [10] Fitch, A.C., Olson, J.B., Lundquist, J.K., Dudhia, J., Gupta, A.K., Michalakes, J., Barstad, I.: Local and mesoscale impacts of wind farms as parameterized in a mesoscale nwp model. *Monthly Weather Review* **140**(9), 3017–3038 (2012)

- [11] Ali, K., Schultz, D.M., Revell, A., Stallard, T., Ouro, P.: Assessment of five wind-farm parameterizations in the weather research and forecasting model: A case study of wind farms in the north sea. *Monthly Weather Review* (2023)
- [12] Platis, A., Siedersleben, S.K., Bange, J., Lampert, A., Bärfuss, K., Hankers, R., Cañadillas, B., Foreman, R., Schulz-Stellenfleth, J., Djath, B., *et al.*: First in situ evidence of wakes in the far field behind offshore wind farms. *Scientific reports* **8**(1), 2163 (2018)
- [13] Lampert, A., Bärfuss, K., Platis, A., Siedersleben, S., Djath, B., Cañadillas, B., Hunger, R., Hankers, R., Bitter, M., Feuerle, T., *et al.*: In situ airborne measurements of atmospheric and sea surface parameters related to offshore wind parks in the german bight. *Earth System Science Data* **12**(2), 935–946 (2020)
- [14] Bärfuss, K., Djath, B., Lampert, A., Schulz-Stellenfleth, J.: Airborne lidar measurements of sea surface properties in the german bight. *IEEE Transactions on Geoscience and Remote Sensing* **59**(6), 4608–4617 (2020)
- [15] Sebastiani, A., Peña, A., Troldborg, N., Meyer Forsting, A.: Evaluation of the global-blockage effect on power performance through simulations and measurements. *Wind Energy Science* **7**(2), 875–886 (2022)
- [16] Schneemann, J., Theuer, F., Rott, A., Dörenkämper, M., Kühn, M.: Offshore wind farm global blockage measured with scanning lidar. *Wind Energy Science* **6**(2), 521–538 (2021)
- [17] Hersbach, H.: Comparison of c-band scatterometer cmod5. n equivalent neutral winds with ecmwf. *Journal of Atmospheric and Oceanic Technology* **27**(4), 721–736 (2010)
- [18] Ahsbahs, T., Badger, M., Volker, P., Hansen, K.S., Hasager, C.B.: Applications of satellite winds for the offshore wind farm site anholt. *Wind Energy Science* **3**(2), 573–588 (2018)
- [19] Christiansen, M.B., Hasager, C.B.: Wake effects of large offshore wind farms identified from satellite sar. *Remote Sensing of Environment* **98**(2–3), 251–268 (2005)
- [20] Nezhad, M.M., Neshat, M., Heydari, A., Razmjoo, A., Piras, G., Garcia, D.A.: A new methodology for offshore wind speed assessment integrating sentinel-1, era-interim and in-situ measurement. *Renewable Energy* **172**, 1301–1313 (2021)
- [21] Schneemann, J., Rott, A., Dörenkämper, M., Steinfeld, G., Kühn, M.: Cluster wakes impact on a far-distant offshore wind farm's power. *Wind*

Energy Science **5**(1), 29–49 (2020)

- [22] Ahsbahs, T., Maclaurin, G., Draxl, C., Jackson, C.R., Monaldo, F., Badger, M.: Us east coast synthetic aperture radar wind atlas for offshore wind energy. Wind Energy Science **5**(3), 1191–1210 (2020)
- [23] Platis, A., Hundhausen, M., Mauz, M., Siedersleben, S., Lampert, A., Bärfuss, K., Djath, B., Schulz-Stellenfleth, J., Cañadillas, B., Neumann, T., *et al.*: Evaluation of a simple analytical model for offshore wind farm wake recovery by in situ data and weather research and forecasting simulations. Wind Energy **24**(3), 212–228 (2021)
- [24] Jiménez, P.A., Navarro, J., Palomares, A.M., Dudhia, J.: Mesoscale modeling of offshore wind turbine wakes at the wind farm resolving scale: A composite-based analysis with the weather research and forecasting model over horns rev. Wind Energy **18**(3), 559–566 (2015)
- [25] Hasager, C.B., Vincent, P., Badger, J., Badger, M., Di Bella, A., Peña, A., Husson, R., Volker, P.J.: Using satellite sar to characterize the wind flow around offshore wind farms. Energies **8**(6), 5413–5439 (2015)
- [26] Cañadillas, B., Foreman, R., Barth, V., Siedersleben, S., Lampert, A., Platis, A., Djath, B., Schulz-Stellenfleth, J., Bange, J., Emeis, S., *et al.*: Offshore wind farm wake recovery: Airborne measurements and its representation in engineering models. Wind Energy **23**(5), 1249–1265 (2020)
- [27] Djath, B., Schulz-Stellenfleth, J., Cañadillas, B.: Impact of atmospheric stability on x-band and c-band synthetic aperture radar imagery of offshore windpark wakes. Journal of Renewable and Sustainable Energy **10**(4), 043301 (2018)
- [28] Pryor, S.C., Barthelmie, R.J., Shepherd, T.J.: Wind power production from very large offshore wind farms. Joule **5**(10), 2663–2686 (2021)
- [29] Stoelinga, M., Sanchez-Gomez, M., Poulos, M.G.S., Crescenti, J., Renewables, A.: Estimating long-range external wake losses in energy yield and operational performance assessments using the wrf wind farm parameterization. Available at: <https://arcvera.com/wp-content/uploads/2022/08/ArcVera-White-Paper-Estimating-Long-Range-External-Wake-Losses-WRF-WFP-1.0.pdf> (2022)
- [30] Cañadillas, B., Beckenbauer, M., Trujillo, J.J., Dörenkämper, M., Foreman, R., Neumann, T., Lampert, A.: Offshore wind farm cluster wakes as observed by long-range-scanning wind lidar measurements and mesoscale modeling. Wind Energy Science **7**(3), 1241–1262 (2022)

- [31] Barthelmie, R.J., Frandsen, S.T., Nielsen, M., Pryor, S., Rethore, P.-E., Jørgensen, H.E.: Modelling and measurements of power losses and turbulence intensity in wind turbine wakes at middelgrunden offshore wind farm. *Wind Energy: An International Journal for Progress and Applications in Wind Power Conversion Technology* **10**(6), 517–528 (2007)
- [32] Owda, A., Badger, M.: Wind speed variation mapped using sar before and after commissioning of offshore wind farms. *Remote Sensing* **14**(6), 1464 (2022)
- [33] Hersbach, H., Bell, B., Berrisford, P., Biavati, G., Horányi, A., Muñoz Sabater, J., Nicolas, J., Peubey, C., Radu, R., Rozum, I., et al.: Era5 hourly data on single levels from 1979 to present. Copernicus climate change service (c3s) climate data store (cds) **10**(10.24381) (2018)
- [34] Hsu, S., Meindl, E.A., Gilhousen, D.B.: Determining the power-law wind-profile exponent under near-neutral stability conditions at sea. *Journal of Applied Meteorology and Climatology* **33**(6), 757–765 (1994)
- [35] Lackner, M.A., Rogers, A.L., Manwell, J.F., McGowan, J.G.: A new method for improved hub height mean wind speed estimates using short-term hub height data. *Renewable Energy* **35**(10), 2340–2347 (2010)
- [36] Atlas, W.: European Wind Atlas (2012)
- [37] Manwell, J.F., McGowan, J.G., Rogers, A.L.: Wind energy explained: theory, design and application (2010)
- [38] Charnock, H.: Wind stress on a water surface. *Quarterly Journal of the Royal Meteorological Society* **81**(350), 639–640 (1955)
- [39] Badger, M., Peña, A., Hahmann, A.N., Mouche, A.A., Hasager, C.B.: Extrapolating satellite winds to turbine operating heights. *Journal of Applied Meteorology and Climatology* **55**(4), 975–991 (2016)
- [40] Skamarock, W.C., Klemp, J.B., Dudhia, J., Gill, D.O., Liu, Z., Berner, J., Wang, W., Powers, J.G., Duda, M.G., Barker, D.M., et al.: A description of the advanced research wrf version 4. NCAR tech. note ncar/tn-556+str **145** (2019)

Table 2: Information about wind farms contained in Fig. 3, including operating country, capacity (MW) and the number of turbines. In total, 52 wind farms related to wake effects (to influence or to be influenced) belonging to six countries (BE, CN, DE, DK, NL and UK) are included, with 3004 turbines and 16.73 GW capacity.

Panel	Number	Wind Farm Name	Country	Capacity (MW)	Turbines
	1	Gemini	NL	600	150
	2				
		Trianel Windpark Borkum 1	DE	200	40
		Trianel Windpark Borkum 2	DE	203	32
	3	Borkum Riffgrund 1	DE	312	78
		Borkum Riffgrund 2	DE	450	56
		Merkur	DE	396	66
a		Alpha Ventus	DE	60	12
		Nordsee One	DE	332.1	54
	4	Gode Wind 1	DE	330	55
		Gode Wind 2	DE	252	42
		Hohe See	DE	497	71
	5	Albatros	DE	112	16
		Global Tech I	DE	400	80
		Meerwind Süd/Ost	DE	288	80
	6	Nordsee Ost	DE	295.2	48
		Kaskasi	DE	342	38
b	1	Hornsea Project One	UK	1218	174
	2	Hornsea Project Two	UK	1386	165
	3	Westermost Rough	UK	210	35
		Humber Gateway	UK	219	73
	1	Inner Dowsing	UK	97.2	27
c	2	Lincs	UK	270	75
	3	Race Bank	UK	573.3	91
	4	Sheringham Shoal	UK	316.8	88
		Dudgeon	UK	402	67
d	1	Datang Jiangsu Binhai	CN	300	95
	2	SPIC Binhai South H3	CN	300	75
	3	SPIC Binhai North H2	CN	400	100
	4	Huaneng Sheyang H1	CN	301.5	67
	5	Longyuan Sheyang H2	CN	301.5	67
	6	SPIC Jiangsu Dafeng H3	CN	302.4	72
		Borssele 1	NL	376	47
		Borssele 2	NL	376	47
e	1	Borssele 3	NL	351.5	37
		Borssele 4	NL	380	40
		Borssele Site V	NL	19	2
		Seamade (Mermaid)	BE	235	28
		Northwester 2	BE	219	23
		Nobelwind	BE	165	50
		Belwind	BE	165	55
	2	Seamade (SeaStar)	BE	252	30
		Northwind	BE	216	72
		Rentel	BE	309	42
		Norther	BE	369.6	44
		Thornton Bank - phase I	BE	30	6
		Thornton Bank - phase II	BE	184.5	30
		Thornton Bank - phase III	BE	110.7	18
	3	East Anglia ONE	UK	714	102
f	1	Horns Rev 2	DK	209.3	91
	2	Horns Rev 3	DK	406.7	49
	3	DanTysk	DE	288	80
	4	Sandbank	DE	288	72